Respiratory Waveform Estimation From Multiple Accelerometers: An Optimal Sensor Number and Placement Analysis

Ailton Siqueira, Jr., Amanda Franco Spirandeli, Raimes Moraes, and Vicente Zarzoso, *Senior Member, IEEE*

***Abstract*—Respiratory patterns are commonly measured to monitor and diagnose cardiovascular, metabolic, and sleep disorders. Electronic devices such as masks used to record respiratory waveforms usually require medical staff support and obstruct the patients' breathing, causing discomfort. New techniques are being investigated to overcome such limitations. An emerging approach involves accelerometers to estimate the respiratory waveform based on chest motion. However, most of the existing techniques employ a single accelerometer placed on an arbitrary thorax position. The present work investigates the use and optimal placement of multiple accelerometers located on the thorax and the abdomen. The study population is composed of 30 healthy volunteers in three different postures. By means of a custom-made microcontrolled system, data are acquired from an array of ten accelerometers located on predefined positions and a pneumotachograph used as reference. The best sensor locations are identified by optimal linear reconstruction of the reference waveform from the accelerometer data in the minimum mean square error sense. The analysis shows that right-hand side locations contribute more often to optimal respiratory waveform estimates, a sound finding given that the right lung has a larger volume than the left lung. In addition, we show that the respiratory waveform can be blindly extracted from the recorded accelerometer data by means of independent component analysis. In conclusion, linear processing of multiple accelerometers in optimal positions can successfully recover respiratory information in clinical settings, where the use of masks may be contraindicated.**

***Index Terms*—Respiratory measurements, accelerometers, linear estimation, minimum mean square error, blind source extraction, independent component analysis.**

Manuscript received January 24, 2018; revised June 24, 2018 and August 9, 2018; accepted August 22, 2018. Date of publication September 3, 2018; date of current version July 1, 2019. The work of A. Siqueira, Jr., was supported by the CAPES-COFECUB project Ma-830-15 "TICoMed.", the work of A. F. Spirandeli was supported by CAPES, and the work of R. Moraes was supported by CNPq (400969/2016-5). V. Zarzoso is a member of the *Institut Universitaire de France. (Corresponding author: Ailton Siqueira, Jr.)*

A. Siqueira, Jr., is with the Departamento de Ciência da Computação, Instituto Federal do Triângulo Mineiro, Ituiutaba 38305-200, Brazil (e-mail: ailton@iftm.edu.br).

A. F. Spirandeli is with the Laboratório de Engenharia Biomédica, Faculdade de Engenharia Elétrica, Universidade Federal de Uberlândia, Uberlândia 38400-902, Brazil (e-mail: amanda.engbiomedica@gmail.com).

R. Moraes is with the Laboratório de Comunicações e Sistemas Embarcados, Universidade Federal de Santa Catarina, Florianópolis 88040-900, Brazil (e-mail: raimes@eel.ufsc.br).

V. Zarzoso is with Université Côte d'Azur, CNRS, I3S Laboratory, 06903 Sophia Antipolis, France (e-mail: zarzoso@i3s.unice.fr).

Digital Object Identifier 10.1109/JBHI.2018.2867727

I. Introduction

RESPIRATORY waveforms assist the diagnosis of cardiorespiratory conditions (such as pneumonia, congestive heart failure, pulmonary embolus, and sleep apnea [1]), the monitoring of patients, and the characterization of toxicological and metabolic emergencies [2]. The post-surgical monitoring of patients respiration allows, for instance, the identification of heart attack imminence associated with a breathing rate above 27 breaths per minute [3].

A medical staff usually measures the respiratory rate by observing abdomen and rib cage movements. However, such a technique is subjective, imprecise, and expensive because it involves a professional dedicated to this task [1], [2], [4]. Alternatively, electronic monitoring of respiratory waveforms typically requires that the patient breathes through apparatuses such as masks or nasal cannulas. Several clinical situations, however, preclude the use of such obstructive devices as they may not be tolerated by critically ill patients [4], [5]. Besides, these devices may affect the respiratory activity and its pattern, biasing the estimation of breathing parameters.

The use of new sensors such as accelerometers may overcome the above limitations by estimating respiratory parameters without obstructing normal breathing [1], [4]–[8]. The basic idea behind this approach is to measure acceleration of thorax walls caused by respiration. Proposed techniques based on accelerometers differ in number of sensors, number of accelerometer axes, acceleration range, used parts, and sensors placement [1], [5], [6], [9]–[17]. However, current investigations do not characterize important aspects related to the use of accelerometers, such as their number and placement on the thorax. Our observations show that a given position may provide signals with different quality (in terms of signal-to-noise ratio, SNR) for different subjects. Hence, it is very likely that different physical characteristics and breathing patterns affect the measurements obtained in different thorax positions; such factors may have a significant impact on respiratory waveform estimation.

To address these limitations, the present work aims to investigate the accelerometer positions that provide sufficient

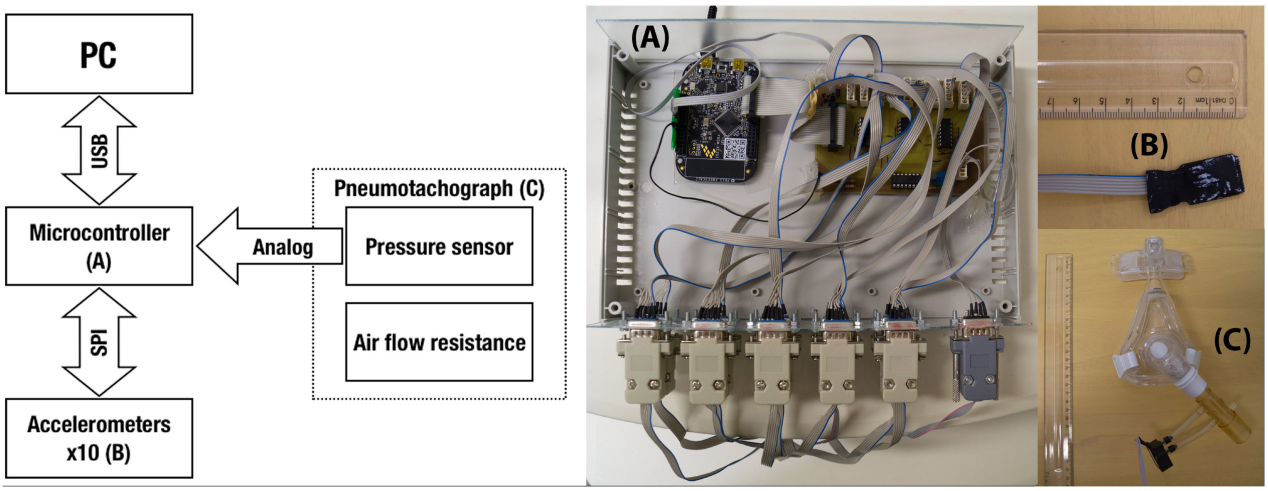

Fig. 1. Block diagram and picture of the developed system, where (A) the microcontroller, (B) an accelerometer, and (C) the pneumotachograph can be seen.

information for a good estimation of the breathing waveform in a heterogeneous population. To this end, a custom-made microcontrolled system is developed to sample data from an array of ten accelerometers placed on the thorax and abdomen as well as from a pneumotachograph mask signal serving as reference. The accelerometer signals are linearly combined to estimate the reference signal by minimizing the mean square reconstruction error. By analyzing all possible combinations of sensor subsets in different subjects, the most frequent locations contributing to optimal reconstructions are adopted as the best accelerometer positions for estimating the respiratory waveform.

The final goal is to avoid obstructive devices in clinical settings where their use may be contraindicated. In such scenarios, no reference signal may be available. We show that the respiratory waveform can be blindly estimated by independent component analysis from four accelerometers placed on the optimal positions found by our analysis.

II. Methods

This section describes the device developed to sample the airflow waveform and the accelerometers signals, the procedure for data acquisition from volunteers, and the digital signal processing techniques used to assess the data.

A. Developed Microcontrolled System

The developed device acquires signals from ten accelerometers and an airflow waveform from a facial mask. Fig. 1 shows a block diagram and a picture of the system.

The accelerometer used is the tri-axial ADXL345 (Analog Devices). It is small (3 mm $\times$ 5 mm $\times$ 1 mm) with a high sensitivity (3.9×10^{-3}g in the least significant bit) which is necessary to register the small displacements of the thorax due to respiration. The ADXL345 contains conditioning circuits, an analog to digital converter (ADC), and serial communication interfaces (SPI and I^2C) to receive configuration commands and transmit the acquired data. In this work, the SPI bus is chosen in order to achieve the desired sampling rate of 80 Hz from each tri-axial accelerometer. The 10 accelerometers share a same SPI bus clocked at 2 MHz; for that, the microcontroller uses additional logic gates (chip select decoder) to address each accelerometer.

The airflow waveform used as reference is obtained by an analog differential pressure transducer (DC030NDC4, Honeywell). This sensor measures the pressure drop across a mechanical resistance (pneumotachograph) that is proportional to the airflow. The pneumotachograph is attached to a facial mask that covers the nose and the mouth of the subject. The bandwidth of the pressure signal is limited to 40 Hz [18] by a second-order Butterworth low-pass filter. The filtered signal is converted to digital by an ADC built in the microcontroller with 16-bit resolution.

The microcontroller used is the ARM Cortex M0+ contained in the FRDM-KL25Z development board (NXP Semiconductors). This microcontroller features all peripherals needed for this application: USB, SPI, ADC, timers, and memories (128 KiB flash; 16 KiB SRAM). The firmware, developed with the MBED Studio Online IDE, controls the data acquisition from the pressure sensor and 10 accelerometers. After each sampling, the data of the 3-axis accelerometers and the pressure transducer are transmitted to a host PC via the USB interface.

Software in the host computer (developed in C#, Microsoft Windows) configures the data acquisition of each accelerometer and defines their measurement ranges (2 g in this work). The parameters specified in the application interface are sent to the FRDM-KL25Z board via USB. The software also shows the waveforms in real-time during the data acquisition and stores the data into files for off-line analysis. The developed device was calibrated and validated by a set of experiments previously reported in [19].

B. Study Population and Data Acquisition

Data were acquired from subjects with no previous history of cardiac or respiratory diseases. The volunteers were informed about the aims and procedures of the investigation and provided written informed consent. The protocol was approved by the Ethics Committee on Human Research of Federal University of Santa Catarina, Florianopolis, Brazil (CAAE no: 53092416.9.0000.0121).

TABLE I
SURVEY OF RESPIRATION MEASUREMENT TECHNIQUES BASED ON ACCELEROMETERS (IN CHRONOLOGICAL ORDER). ICS: INTERCOSTAL SPACE; —: NOT INFORMED

Reference	Accelerometers				
	Number	Axes	Range	Part	Placement
Reinvuo [9]	2	1	2g	SCA620	Sternum, heart, processus xiphoideus, solar plexus
Phan [10]	2	2	1.7g	ADXL204	Around the heart and the thorax
Jin [11]	1	3	—	—	Below the xiphoid process
Bates [1], [12]	1	3	1.5g	MMA7260QT	Left lower costal margin
Chan [5], [13], [14]	1	3	4g	—	2nd ICS, vertically over the sternum, 6th or 7th ICS
Lapi [4]	2	3	—	—	10th rib
Estrada [15]	2	3	2g	8312B2	Between 7th and 8th ICS
Fekr [6], [7], [8], [16]	2	3	2g	LIS3DH	Middle sternum and abdomen
Zhang [17]	1	3	—	—	Heart

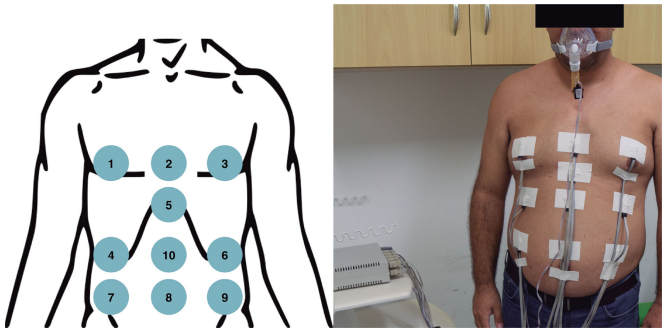

Fig. 2. Accelerometer positions and picture of the experimental setup.

A survey was carried out to find out the measuring range, number and placement of accelerometers used in previous works. A summary is given in Table I. To investigate the best locations for the transducers that lead to good quality signals from different subjects, the 10 accelerometers were placed in positions pointed out by the survey. Fig. 2 shows the chosen positions. The accelerometer array was disposed across a 3×3 grid with an extra location on the xiphoid process (sensor 5). The accelerometers 1, 2, and 3 were placed on the middle of the chest using the nipples as landmark. Accelerometers 4, 5, and 6 were on the costal arch. Sensors 7, 8, and 9 were placed on the middle of the abdomen, using the belly button as reference. The last sensor (10) was also placed on the abdomen, at the same height of accelerometers 4 and 6, below sensor 5. The volunteers also wore a facial mask connected to the differential pressure transducer that registered the airflow waveform used as reference.

Each subject participated in three recording sessions corresponding to different postures: standing, sitting, and lying in supine position. Throughout the acquisition protocol, subjects were asked to breathe as they felt most comfortable (spontaneous breathing). Each session lasted 6 minutes, with a minimum resting interval of 30 seconds between sessions.

C. Data Preprocessing

The sampled accelerometer data contain relative high frequency noise as well as an offset due to gravity. The signals acquired by the accelerometers are therefore filtered and detrended to remove these components. A type-II Chebyshev lowpass filter with 5-Hz cutoff frequency and 60-dB stopband attenuation is first applied. The signals are forward and reverse filtered to avoid phase distortions. Next, the offset and low frequency components are removed by linear detrending of consecutive 30-s segments using standard Matlab functions. The same preprocessing steps are applied on the airflow waveform to ensure an agreement with the accelerometer data in terms of spectral density.

The resulting airflow signal after preprocessing is denoted $b(n)$, with $n = 0, 1, \ldots, (N-1)$ representing the sample index, where $N = 28800$ samples in the 6-minute long recorded data segment. The kth accelerometer, $k = 1, 2, \ldots, 10$, provides three signals $a_{k,x}(n)$, $a_{k,y}(n)$, $a_{k,z}(n)$, corresponding to the acceleration measured along three orthogonal directions. At each sample index, the accelerometer data can conveniently be stored in a 30-dimensional vector

$$\mathbf{a}(n) = [a_{1,x}(n), a_{1,y}(n), a_{1,z}(n), \ldots, a_{10,x}(n), a_{10,y}(n), a_{10,z}(n)]^{\mathrm{T}} \quad (1)$$

where symbol $(\cdot)^{\mathrm{T}}$ denotes the matrix transpose operator.

D. Minimum Mean Square Error (MMSE) Estimation

The number of accelerometers and their best positions for breathing waveform estimation are assessed by means of the minimum mean square error (MMSE) approach as described in this section. Modern digital signal processing techniques applied to communications, speech recognition, robotics, automatic control, and biomedical engineering usually comprise linear parametric estimation [20], especially when multiple transducers are employed, giving rise to the so-called multiple-input multiple-output (MIMO) systems [21], [22]. A classical example where linear estimation proves useful is channel equalization in digital communication systems, when the transmission of training symbols can be used as reference signals by the receiver.

Inspired by this approach, we assume in this work that the breathing waveform can be derived from a noisy linear combination of accelerometer outputs, according to the signal model:

$$b(n-d) = \mathbf{c}^{\mathrm{T}}\mathbf{a}(n) + w(n) \quad (2)$$

where vector $\mathbf{c}$ contains the linear combination coefficients and $w(n)$ represents the additive noise. Model (2) explicitly takes into account the presence of a time delay of d samples between the accelerometer and airflow waveforms. Indeed, the thorax expansion, promptly registered by the accelerometers, causes a negative pressure within the lungs that generates the airflow detected by the pressure transducer; the opposite occurs during expiration.

Assuming a fixed value of d, the optimal linear combination coefficients can be determined by maximizing the expected log-likelihood of the observations. Under additive white Gaussian noise, this approach leads to the MMSE estimator:

$$\hat{\mathbf{c}}_{\mathrm{MMSE}}(d) = \arg\min_{\mathbf{c}} \mathrm{E}\{[\mathbf{c}^{\mathrm{T}}\mathbf{a}(n) - b(n-d)]^2\}$$

where $\mathrm{E}\{\cdot\}$ represents the mathematical expectation operator. In practice, the mathematical expectation is replaced by time averaging over the available samples, and the MMSE estimator can be formulated as the least squares problem:

$$\hat{\mathbf{c}}_{\mathrm{MMSE}}(d) = \arg\min_{\mathbf{c}} \|\mathbf{A}\mathbf{c} - \mathbf{b}_d\|^2 \tag{3}$$

where

$$\mathbf{A} = [\mathbf{a}(0), \mathbf{a}(1), \ldots, \mathbf{a}(N-1)]^{\mathrm{T}} \tag{4}$$

represents the accelerometer data matrix, with dimensions $(N \times 30)$, and $\mathbf{b}_d = [b(-d), b(1-d), \ldots, b(N-1-d)]^{\mathrm{T}}$. Symbol $\|\cdot\|$ denotes the classical Euclidean ℓ_2-norm. The solution to problem (3) is well known (see, e.g., [20]) and is readily given by

$$\hat{\mathbf{c}}_{\mathrm{MMSE}}(d) = (\mathbf{A}^{\mathrm{T}}\mathbf{A})^{-1}\mathbf{A}^{\mathrm{T}}\mathbf{b}_d$$

and the MMSE can be expressed, up to an irrelevant scale factor, as

$$\varepsilon(d) = \|\mathbf{b}_d\|^2 - \mathbf{b}_d^{\mathrm{T}}\mathbf{A}(\mathbf{A}^{\mathrm{T}}\mathbf{A})^{-1}\mathbf{A}^{\mathrm{T}}\mathbf{b}_d. \tag{5}$$

The optimum delay is estimated as the value of d yielding the lowest MMSE:

$$\hat{d}_{\mathrm{opt}} = \arg\min_{d} \varepsilon(d).$$

To determine $\hat{d}_{\mathrm{opt}}$, we perform an exhaustive grid search over a $\pm$5-s interval ($\pm$400 samples) around $d = 0$. According to model (2), the final MMSE estimate of the airflow signal can be obtained as

$$\hat{b}(n - \hat{d}_{\mathrm{opt}}) = \mathbf{c}^{\mathrm{T}}\mathbf{a}(n) \tag{6}$$

with $\mathbf{c} = \hat{\mathbf{c}}_{\mathrm{MMSE}}(\hat{d}_{\mathrm{opt}})$. As a performance index, we compute the normalized mean square error (NMSE), defined as:

$$\mathrm{NMSE} = \frac{\mathrm{E}\{[\hat{b}(n) - b(n)]^2\}}{\mathrm{E}\{b(n)^2\}} \tag{7}$$

which for the MMSE estimator can also be expressed as

$$\mathrm{NMSE} = \frac{\varepsilon(\hat{d}_{\mathrm{opt}})}{\|\mathbf{b}_0\|^2}. \tag{8}$$

Finally, remark that to compute solution (3), the accelerometer data matrix $\mathbf{A}$ is only required to be full column rank, which is likely to occur in most experimental conditions where $N \gg 30$.

E. Optimal Sensor Number and Placement Analysis

To find the most suitable number of sensors and their best locations, we adopt a combinatorial approach using different subsets of K accelerometers placed as in Fig. 2, with K ranging from 1 to 10. For a given combination of K accelerometers, the breathing waveform is estimated by the above MMSE-based procedure. To do so, one just needs to retain the $3K$ entries of vector $\mathbf{a}$ in Equation (1) and columns of matrix $\mathbf{A}$ in Equation (4) corresponding to the tri-axial sensor subset under analysis. The resulting matrix $\mathbf{A}$ has dimensions $(N \times 3K)$. The NMSE can be computed from Equations (5) and (8). All possible combinations of K accelerometers can be considered in this manner.

For a given value of K, a total of $\binom{10}{K} = \frac{10!}{K!(10-K)!}$ different combinations are available. To detect whether the estimation error decreases significantly as more accelerometers are included, NMSE distributions for two consecutive values of K can then be compared by suitable statistical tests. After testing distribution normality with Lilliefors test, a Student t-test is applied if the data are Gaussian, a Mann-Whitney U-test otherwise. For each K, the accelerometers contributing to the combination yielding the minimum NMSE are noted for each subject. The accelerometers appearing more frequently are considered to be indicative of optimal sensor locations. A maximum value of $K = 5$ was chosen in this analysis because such a value provides the highest number of combinations, $\binom{10}{5} = 252$, for the available set of accelerometers, and higher values of K naturally increase the number of sensors in the optimal combination, and thus, the chances of obtaining spurious locations. This optimal sensor placement analysis is repeated for each breathing posture (standing, sitting, lying).

F. Blind Extraction of the Respiratory Signal

The optimal sensor number and placement analysis described above is based on a mask signal, which, as explained in the Introduction, may be contraindicated for certain patients and would actually make unnecessary the use of alternative sensors such as accelerometers. To highlight the clinical interest of accelerometers, the second main goal of the present work is to demonstrate that respiratory information can be extracted from accelerometer arrays blindly, i.e., without the use of additional devices, obstructive or otherwise, providing reference information.

To this end, we make the assumption that the accelerometer signals arise as unknown linear combinations of the desired breathing signal and other sources of physiological activity and artefacts. As a result of this hypothesis, the accelerometer output vector (1) can be modeled as a blind source separation (BSS) problem:

$$\mathbf{a}(n) = \mathbf{H}\mathbf{s}(n) \tag{9}$$

where vector $\mathbf{s}(n)$ contains the source signals, including breathing, artefacts and noise, and $\mathbf{H}$ stands for the unknown mixing matrix, whose entries model the contribution of each source signal in vector $\mathbf{s}(n)$ to each observation in vector $\mathbf{a}(n)$. BSS aims at the unsupervised estimation of the original waveforms $\mathbf{s}(n)$ from their observed mixtures $\mathbf{a}(n)$. If mixing matrix $\mathbf{H}$ is full column rank, the source signals can be obtained by estimating its inverse $\mathbf{H}^{-1}$, whose rows define how the observed signals must be linearly combined to estimate the sources. Therefore, a source signal can be recovered by applying a linear extractor $\mathbf{w}$ onto the observed vector:

$$\hat{s}(n) = \mathbf{w}^{\mathrm{T}}\mathbf{a}(n) \tag{10}$$

symbol $(\cdot)^{\mathrm{T}}$ denoting the matrix transpose operator. To determine source extractors, BSS techniques maximize suitable contrast functions of the extractor output $\hat{s}$ measuring a known property of the sources. In many applications, the sources are mutually independent and one can maximize related nongaussianity indices such as kurtosis. This idea is the basis of independent component analysis (ICA), the most popular tool for BSS of independent components. A comprehensive account of BSS and ICA, including biomedical applications, can be found in the reference book [23]. In our particular problem, breathing can be considered statistically independent of other sources of physiological activity, artefacts and measurement noise. Thus, ICA arises as a suitable approach for the blind extraction of respiratory patterns according to BSS model (9).

In this work, the RobustICA algorithm [24] estimates the extracting vector from accelerometer signals by searching for the global optima of the kurtosis contrast. Details of this algorithm can be found in [24] and a Matlab implementation is available in [25]. Since respiratory signals resemble sinusoidal waves, characterized by negative kurtosis values, we configure RobustICA to search for a subgaussian component. After convergence of the algorithm, the obtained extracting vector can estimate the respiratory waveform according to Equation (10), without the need for a facial mask or any other reference signal.

For the quantitative assessment of the recovered respiratory waveform, its NMSE relative to the gold standard (facial mask waveform) is computed after correcting for the amplitude and phase ambiguities inherent to blind techniques. To do so, the extracted subgaussian independent component is first scaled by factor

$$\alpha = \sqrt{\frac{\mathrm{E}\{b^2\}}{\mathrm{E}\{\hat{b}^2\}}}$$

to obtain the same power level as the mask airflow reference. To find out the time delay between the two signals, the maximum absolute cross-correlation is sought by an exhaustive grid search within a ± 500 samples window. The estimated component is inverted if the cross-correlation at the computed time delay is negative. Once the independent component is corrected, the NMSE can finally be computed as in Equation (7).

III. Results

A. Study Population

Thirty male healthy subjects participated in the study. Table II presents the participants' anthropometric data.

TABLE II
ANTHROPOMETRIC CHARACTERISTICS OF THE STUDY POPULATION

ID	Age	Height (m)	Weight (kg)	Chest (m)	Abdomen (m)
1	52	1.74	76.0	0.91	0.95
2	31	1.78	83.3	1.02	0.90
3	32	1.73	61.3	0.86	0.77
4	28	1.78	84.8	1.06	0.94
5	32	1.79	91.5	1.06	0.94
6	35	1.65	64.8	0.88	0.80
7	27	1.71	72.0	0.97	0.84
8	37	1.69	96.6	1.08	1.12
9	23	1.81	77.7	0.97	0.80
10	33	1.82	108.5	1.05	1.11
11	29	1.80	83.9	0.91	0.88
12	26	1.75	72.4	0.93	0.80
13	20	1.70	76.7	0.98	0.87
14	25	1.90	97.3	1.02	0.95
15	23	1.72	75.5	0.96	0.82
16	31	1.80	79.0	0.95	0.86
17	21	1.80	82.6	1.00	0.88
18	21	1.83	81.6	0.98	0.86
19	18	1.74	71.0	0.94	0.80
20	19	1.84	78.1	0.98	0.84
21	23	1.93	75.2	0.91	0.83
22	18	1.80	69.9	0.93	0.76
23	19	1.78	74.3	0.93	0.84
24	18	1.77	69.8	0.92	0.81
25	50	1.69	75.0	1.00	0.95
26	37	1.80	116.9	1.20	1.14
27	66	1.68	103.0	1.13	1.21
28	21	1.79	69.6	0.91	0.86
29	19	1.72	73.8	0.89	0.83
30	23	1.70	64.1	0.85	0.80
Mean	29	1.77	80.2	0.97	0.89
Std.	11.22	0,06	13.1	0.08	0.12
Max	66	1.93	116.9	1.20	1.21
Min	18	1.65	61.3	0.85	0.76

B. Optimal Sensor Number and Placement

Fig. 3 shows the NMSE box plot for all possible combinations of accelerometer subsets over all subjects. A decreasing median and variability of the error can be clearly observed when more accelerometers are used in the estimation. This outcome is obtained for the three postures. The p-values between NMSE distributions for consecutive values of K are shown for the last three comparisons ($K = 7$ vs. $K = 8$, $K = 8$ vs. $K = 9$ and $K = 9$ vs. $K = 10$). For the sake of clarity, the remaining comparisons are omitted as they present very small p-values in all cases.

The NMSE trends in Fig. 3 show that the error does not decrease significantly when the number of sensors is increased above eight. Besides, a proper choice of sensor placement may allow the acquisition of signals using smaller arrays, simplifying the hardware. To check this hypothesis, sensor combinations achieving the best estimates are identified as explained in Section II-E. Table III gives an example of the optimal sensor placement results for two different subjects in the sitting posture. The first column identifies the volunteer; the second one shows the number of accelerometers in the subset, and the remaining columns inform whether the corresponding accelerometer is used (value 1) or not (value 0) to achieve the best linear estimate of the mask reference signal for that particular subject. The bottom row counts the number of times that a given position contributed to optimal estimates.

By repeating this procedure for all subjects, the occurrences of each accelerometer position can be summarized as in Fig. 4. At each accelerometer position, a circle is drawn with radius proportional to the overall incidence of that position in the sensor combination achieving the best respiratory waveform estimate across volunteers. Accordingly, larger circles indicate accelerometers appearing more frequently in subsets yielding the best estimates. Fig. 4 shows that accelerometers 4, 5, and 7 appear more often in the best estimates. Accelerometers 2,

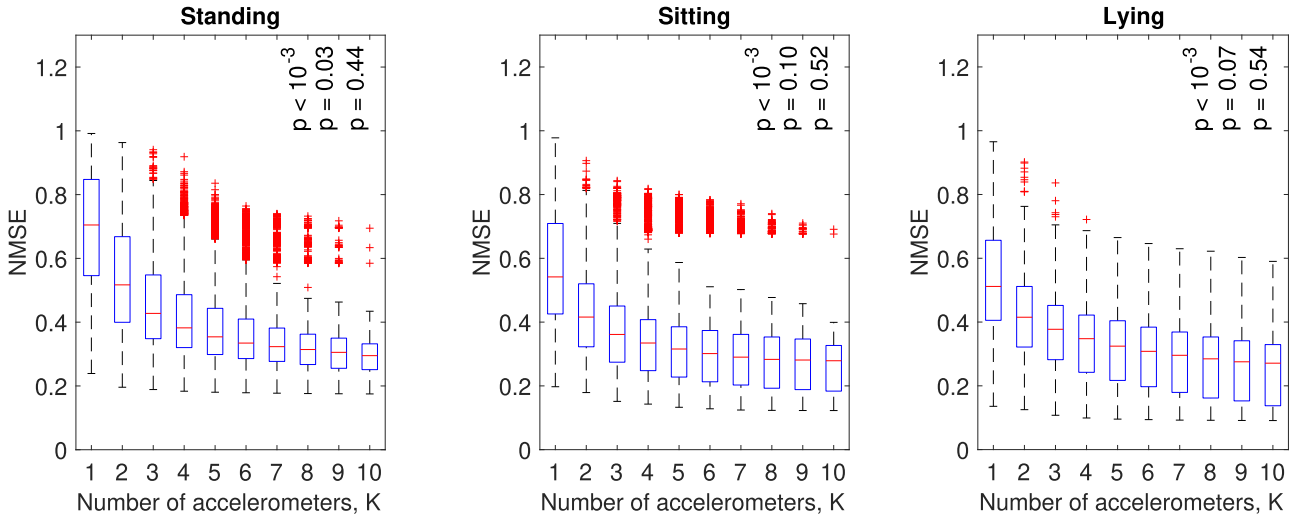

Fig. 3. Performance variation of the MMSE estimator with the number of accelerometers used to reconstruct the breathing waveform.

TABLE III
ILLUSTRATIVE EXAMPLE OF OPTIMAL SENSOR ASSESSMENT FOR TWO DIFFERENT SUBJECTS IN THE SITTING POSTURE. K: NUMBER OF ACCELEROMETERS

		Position									
Subject	K	1	2	3	4	5	6	7	8	9	10
2	1	0	0	0	0	0	0	0	1	0	0
	2	0	0	0	1	0	0	1	0	0	0
	3	0	0	0	1	0	0	1	0	1	0
	4	0	0	0	1	0	1	1	0	1	0
	5	0	0	1	1	0	1	1	0	1	0
7	1	0	0	0	0	1	0	0	0	0	0
	2	0	0	0	0	1	0	0	1	0	0
	3	0	0	0	1	1	0	1	0	0	0
	4	0	1	0	1	1	0	1	0	0	0
	5	0	1	1	1	1	0	1	0	0	0
	Ocurrences	0	2	2	7	5	2	7	2	3	0

6, 8, 9, and 10 occur less often, indicating that they seem to contribute less significantly to optimal sensor combinations.

One can also remark that the accelerometers placed on the right-hand side contribute more frequently than those on the left-hand side. To quantify this observation, the difference in reconstructed NMSE between the accelerometers placed on the left (positions 3, 6, and 9) and on the right (positions 1, 4, and 7) is assessed by appropriate statistical tests. Fig. 5 shows that right-hand side accelerometers yield indeed significantly lower NMSE values than those located on the left-hand side for the three postures. The p-values are obtained by Student t-tests after confirming data normality.

C. Blind Extraction of Respiratory Signal

After identifying the positions containing more information, breathing waveforms recovered by RobustICA (Section II-F) and MMSE are compared to the reference ones (pneumotacograph). For each posture, the comparisons are carried out using waveforms obtained from two different sets of accelerometers as shown in Table IV. These two sets of accelerometers correspond to the best 4 and the best 8 positions in Fig. 4.

Fig. 6 shows an example of these estimations and Fig. 7 compares the NMSE for the two estimators (RobustICA and MMSE) and two sets of sensors. All waveforms are scaled and synchronized (as already described) before computing the NMSE. There are some outliers that will be addressed on the discussion section. For all postures and both estimators, statistical tests show no differences between the NMSE obtained from the two sets (p-values are presented above the corresponding box plots). Fig. 7 shows that the NMSE is higher for the RobustICA than for MMSE, as expected, but they present the same order of magnitude. Fig. 7 also shows that a set of 4 accelerometers allows the recovery of a breathing waveform similar to that obtained from a set of 8 sensors (no statistical difference). RobustICA succeeded in finding good breathing waveform estimates in the first independent component extracted from a set of 4 accelerometers.

IV. DISCUSSION

The present work shows that respiratory information can be recovered by using multiple tri-axial accelerometers located on the subject's thorax and abdomen. The developed hardware system allows us to assess the use of multiple (up to ten) sensors to estimate the breathing waveform. In contrast to previous works requiring nonlinear processing, respiratory information can be obtained by linearly combining the acquired accelerometer signals as in Equation (6). Some salient results are discussed next.

A. Interest of Multiple Accelerometers

A combinatorial analysis is employed to investigate the effects of the number of accelerometers as well as their optimal placement on the thorax and abdomen. As the number of accelerometers increases, the reference mask signal can be approximated with increasing accuracy in the NMSE sense (Fig. 3). Therefore, multiple spatially separated sensors can be used to acquire signals with improved SNR. In contrast, previous works did not use more than two accelerometers to estimate the respiratory waveform (Table I). Estimation quality is enhanced

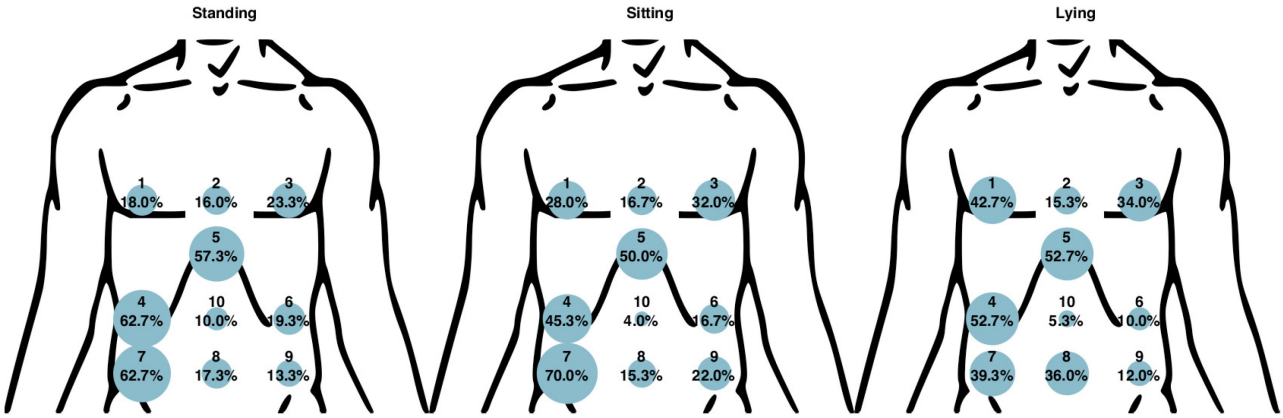

Fig. 4. Percentage of occurrences of each accelerometer in the combinations with the lowest NMSE. Accelerometer numbers correspond to the positions shown in Fig. 2.

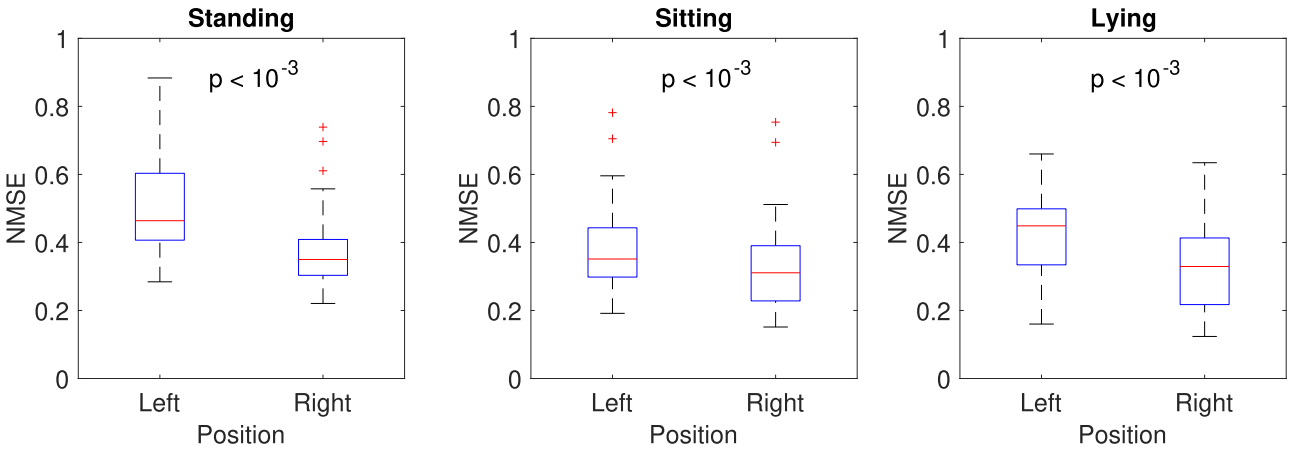

Fig. 5. Airflow signal reconstruction error from accelerometers located on the left and on the right side of the body.

TABLE IV
SETS OF 4 AND 8 ACCELEROMETERS USED TO COMPARE THE WAVEFORMS OBTAINED BY ROBUSTICA AND MMSE IN Fig. 7. THESE SETS CORRESPOND TO THE OPTIMAL POSITIONS SHOWN IN Fig. 4

Posture	Set 1 (4 Accelerometers)	Set 2 (8 Accelerometers)
Standing	3, 4, 5, 7	1, 2, 3, 4, 5, 6, 7, 8
Sitting	3, 4, 5, 7	1, 2, 3, 4, 5, 6, 7, 9
Lying	1, 4, 5, 7	1, 2, 3, 4, 5, 7, 8, 9

in a statistically significant manner as the number of accelerometer increases up to eight, whereas a larger number of sensors does not seem to provide substantial improvements (Fig. 3).

B. Optimal Sensor Placement, Right vs. Left Side

Respiratory waveform estimation performance also depends on sensor placement. In the three breathing postures under test, accelerometers placed on the right-hand side contribute more often to the optimal MMSE estimate among all possible sensor combinations. This previously unnoticed outcome is consistent with anatomy, since the lungs are asymmetric: the right lung has a larger volume than the left one [26]. Differences between the left and right side were also reported in previous chest

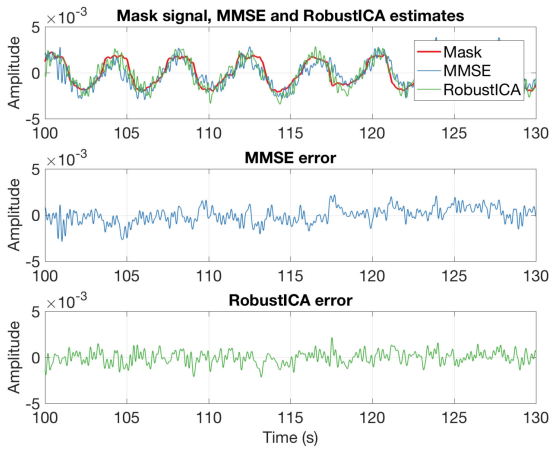

Fig. 6. Example of a reference mask signal and the obtained MMSE and RobustICA estimates using four accelerometers (top), together with the respective error signals (MMSE residual, middle; RobustICA residual, bottom).

wall motion studies [27]. Hence, it is sensible to infer that the right lung walls experience larger displacements during respiration, and therefore produce more pronounced effects

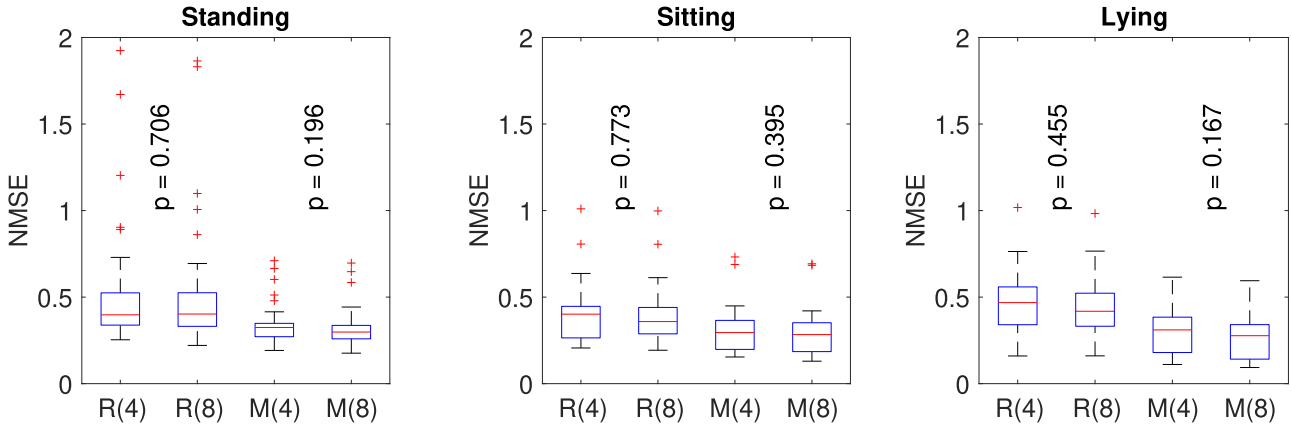

Fig. 7. Airflow signal estimation results by supervised (MMSE - M) and unsupervised (RobustICA - R) methods for the three breathing postures. Estimations are obtained from the optimal sets of 4 or 8 accelerometers (in parentheses), which are detailed in Table IV.

on the accelerometer outputs. These outputs, in turn, present stronger correlations with the airflow signal and contribute more easily to the optimal linear estimate.

We could also observe that a proper choice of accelerometer positions influences the quality of the estimation. Section III-B stated that performance improves using up to eight accelerometers when considering all possible combinations of the ten sensor positions under study. According to further analysis (Section III-C), the optimal positions (Fig. 4) lead to a breathing waveform estimation using 4 sensors with no significant difference from that obtained using 8 sensors (Fig. 7).

Most authors placed the accelerometers on the middle and left side (Table I). It is likely that they would get better results placing the sensors on the right side. Our results indicate that positions 4 and 7 (Fig. 4) should be employed to estimate respiratory waveforms in the three postures considered in this work. In addition, the sensor placed on the xiphoid process (position 5) also stands out.

C. Blind Processing

In most of our experiments, the respiratory waveform was successfully blindly recovered by the RobustICA algorithm using four or eight accelerometers in the positions determined by our optimal location analysis (Figs. 6–7). The respiratory signal is consistently found in the first extracted independent component when the algorithm is configured to target subgaussian sources. This positive result further supports the pertinence of linear model (2) and linear estimate (6) assumed in our analysis and demonstrates the applicability of the proposed approach in clinical settings where the use of obstructing devices may be contraindicated.

This part of the study did not mean to show the superiority of RobustICA over alternative ICA or source separation methods, but simply the suitability of ICA as a blind estimator of respiration from accelerometer data. This general purpose independent source extraction technique was selected for its satisfactory performance on biomedical data reported in previous works (e.g. [24]), and further improvements may be obtained by specific adaptations to the problem under study. In particular, RobustICA failed in cases where the recorded SNR was rather low, probably due to poor accelerometer contact. Accordingly, the impact of outliers could be reduced by paying more attention to sensor contact or designing novel blind extraction techniques capable of handling noisy records in this application.

This part of the work was intended as a proof of concept that respiratory waveforms can be blindly recovered from the sensor array output, supporting the clinical interest of accelerometers for breathing parameter estimation. Blind processing was limited to the four and eight optimal sensor locations in each body posture because our goal was simply to demonstrate that breathing information can be extracted without mask reference from accelerometer arrays, even with simplified hardware composed of a reduced number of sensors. A more detailed analysis of the influence of accelerometer array size on blind extraction performance is left for further investigations.

D. Study Limitations

Only healthy subjects are considered in our study. Respiratory pathologies that could lead to different results shall be addressed by further research. The potential influence of breasts on respiratory estimation from chest accelerometers has been avoided by limiting the analysis to a male population, and should be considered in further studies by including female subjects. The proposed approach has not been compared with existing techniques because emphasis has been laid on the analysis of optimal sensor number and placement rather than on the comparative performance of different methods. Also, the protocol based on sensor locations constrained to a predefined grid precludes the comparison with alternative techniques relying on other accelerometer positions, as the developed hardware can not support additional sensors.

V. Conclusion

The present work has shown that respiratory information in different breathing postures can be estimated by multiple tri-axial accelerometers located on the subject's thorax and abdomen. To our knowledge, this is the first study addressing

the question of the optimal number and placement of sensors through a systematic analysis. The developed custom-made hardware can record and analyze signals from up to ten accelerometers and a reference airflow waveform. As opposed to previous approaches based on some sort of nonlinear processing or transformation, respiratory information can be estimated by linearly combining the recorded accelerometer outputs. As the number of accelerometers increases, the reference airflow signal can be approximated with increasing accuracy, thus demonstrating the interest of using multiple spatially separated sensors. In the combinatorial MMSE analysis, the right costal arch appears as the best location for accelerometer placement, in coherence with the larger volume of the right lung. Respiratory information can also be recovered blindly, i.e., without the use of a mask reference signal, by means of source separation techniques such as RobustICA, which demonstrates the usefulness of this approach in clinical environments where obstructive devices may not be recommended. These results open interesting new perspectives for the use of accelerometers to estimate respiratory information in widespread clinical practice and body sensor networks.

Further work should consider databases including female subjects and respiratory pathologies, and compare the proposed approach with alternative techniques for respiratory signal estimation.

Acknowledgment

The authors would like to thank all the volunteers that kindly participated in the experiments as well as the anonymous reviewers whose comments on the original manuscript helped to improve the paper.

References

[1] A. Bates, M. J. Ling, J. Mann, and D. K. Arvind, "Respiratory rate and flow waveform estimation from tri-axial accelerometer data," in *Proc. Int. Conf. Body Sens. Netw.*, Singapore, Jun. 2010, pp. 144–150.

[2] P. B. Lovett, J. M. Buchwald, K. Stürmann, and P. Bijur, "The vexatious vital: Neither clinical measurements by nurses nor an electronic monitor provides accurate measurements of respiratory rate in triage," *Ann. Emergency Med.*, vol. 45, no. 1, pp. 68–76, Jan. 2005.

[3] I. Smith, J. Mackay, N. Fahrid, and D. Krucheck, "Respiratory rate measurement: A comparison of methods," *Brit. J. Healthcare Assistants*, vol. 5, no. 1, pp. 18–23, Jan. 2011.

[4] S. Lapi *et al.*, "Respiratory rate assessments using a dual-accelerometer device," *Respiratory Physiol. Neurobiol.*, vol. 191, no. 1, pp. 60–66, Jan. 2014.

[5] A. M. Chan, N. Ferdosi, and R. Narasimhan, "Ambulatory respiratory rate detection using ECG and a triaxial accelerometer," in *Proc. Annu. Int. Conf. IEEE Eng. Med. Biol. Soc.*, Osaka, Japan, Jul. 2013, pp. 4058–4061.

[6] A. R. Fekr, K. Radecka, and Z. Zilic, "Tidal volume variability and respiration rate estimation using a wearable accelerometer sensor," in *Proc. 4th Int. Conf. Wireless Mobile Commun. Healthcare*, Athens, Greece, Nov. 2014, pp. 1–6.

[7] A. R. Fekr, K. Radecka, and Z. Zilic, "Design and evaluation of an intelligent remote tidal volume variability monitoring system in e-health applications," *IEEE J. Biomed. Health Inform.*, vol. 19, no. 5, pp. 1532–1548, Jun. 2015.

[8] A. R. Fekr, M. Janidarmian, K. Radecka, and Z. Zilic, "Respiration disorders classification with informative features for m-health applications," *IEEE J. Biomed. Health Inform.*, vol. 20, no. 3, pp. 733–747, May 2016.

[9] T. Reinvuo, M. Hannula, H. Sorvoja, E. Alasaarela, and R. Myllyla, "Measurement of respiratory rate with high-resolution accelerometer and EMFit pressure sensor," in *Proc. IEEE Sens. Appl. Symp.*, Houston, TX, USA, Feb. 2006, pp. 192–195.

[10] J. Mann, R. Rabinovich, A. Bates, S. Giavedoni, W. MacNee, and D. K. Arvind, "Simultaneous activity and respiratory monitoring using an accelerometer," in *Proc. Int. Conf. Body Sens. Netw.*, Dallas, TX, USA, May 2011, pp. 139–143.

[11] A. Jin, B. Yin, G. Morren, H. Duric, and R. M. Aarts, "Performance evaluation of a tri-axial accelerometry-based respiration monitoring for ambient assisted living," in *Proc. Annu. Int. Conf. IEEE Eng. Med. Bol. Soc.*, Minneapolis, MN, USA, Sep. 2009, pp. 5677–5680.

[12] G. B. Drummond, A. Bates, J. Mann, and D. K. Arvind, "Validation of a new non-invasive automatic monitor of respiratory rate for post-operative subjects," *Brit. J. Anaesthesia*, vol. 107, no. 3, pp. 462–469, Sep. 2011.

[13] A. M. Chan, N. Selvaraj, N. Ferdosi, and R. Narasimhan, "Wireless patch sensor for remote monitoring of heart rate, respiration, activity, and falls," in *Proc. Annu. Int. Conf. IEEE Eng. Med. Biol. Soc.*, Osaka, Japan, Jul. 2013, pp. 6115–6118.

[14] A. Chan and R. Narasimhan, "Respiratory rate measurement using a combination of respiration signals," U.S. Patent 20 140 228 692, Aug. 2014. [Online]. Available: http://www.google.com/patents/US20140228692

[15] L. Estrada, A. Torres, L. Sarlabous, J. A. Fiz, and R. Jané, "Respiratory rate detection by empirical mode decomposition method applied to diaphragm mechanomyographic signals," in *Proc. Annu. Conf. IEEE Eng. Med. Biol. Soc.*, Chicago, IL, USA, Aug. 2014, pp. 3204–3207.

[16] A. R. Fekr, M. Janidarmian, K. Radecka, and Z. Zilic, "A medical cloud-based platform for respiration rate measurement and hierarchical classification of breath disorders," *Sensors*, vol. 14, no. 6, pp. 11 204–11 224, Jun. 2014.

[17] Z. Zhang and G.-Z. Yang, "Monitoring cardio-respiratory and posture movements during sleep: What can be achieved by a single motion sensor," in *Proc. 12th IEEE Int. Conf. Wearable Implantable Body Sens. Netw.*, Cambridge, MA, USA, Jun. 2015, pp. 1–6.

[18] F. P. Primiano, Jr., "Measurements of the respiratory system," in *Medical Instrumentation: Application and Design*, 4th ed., J. G. Webster, Ed. Hoboken, NJ, USA: Wiley, 2010, ch. 9, pp. 377–448.

[19] A. L. D. Siqueira Jr., T. F. Rech, R. Moraes, and V. Zarzoso, "Desenvolvimento de monitor respiratório utilizando múltiplos acelerômetros," in *Proc. XXV Brazilian Congr. Biomed. Eng.*, Foz do Iguaçu, Brazil, Oct. 2016, pp. 627–630.

[20] A. Cichocki and S. Amari, *Adaptive Blind Signal and Image Processing*. Chichester, U.K.: Wiley, 2002.

[21] V. Zarzoso and A. K. Nandi, "Blind MIMO equalization with optimum delay using independent component analysis," *Int. J. Adaptive Control Signal Process.*, vol. 18, no. 3, pp. 245–263, Apr. 2004.

[22] Z. Ge and W. Haiyan, "Linear precoding design for massive MIMO based on the minimum mean square error algorithm," *EURASIP J. Embedded Syst.*, vol. 2017, no. 20, pp. 1–6, Jan. 2017.

[23] P. Comon and C. Jutten, Eds., *Handbook of Blind Source Separation, Independent Component Analysis and Applications*. Oxford, U.K.: Academic, 2010.

[24] V. Zarzoso and P. Comon, "Robust independent component analysis by iterative maximization of the kurtosis contrast with algebraic optimal step size," *IEEE Trans. Neural Netw.*, vol. 21, no. 2, pp. 248–261, Feb. 2010.

[25] RobustICA package, Nov. 2014. [Online]. Available: www.i3s.unice.fr/~zarzoso/robustica.html

[26] B. Johansen, O. Bjørtuft, and J. Boe, "Static lung volumes in healthy subjects assessed by helium dilution during occlusion of one mainstem bronchus," *Thorax*, vol. 48, no. 4, pp. 381–384, Apr. 1993.

[27] A. De Groote, M. Wantier, G. Cheron, M. Estenne, and M. Paiva, "Chest wall motion during tidal breathing," *J. Appl. Physiol.*, vol. 83, no. 5, pp. 1531–1537, 1997.